Construction and Building Materials 233 (2020) 117352

Contents lists available at ScienceDirect

Construction and Building Materials

journal homepage: www.elsevier.com/locate/conbuildmat

Pavement-distress detection using ground-penetrating radar and network in networks

Zheng Tong [a,d,**], Dongdong Yuan [b], Jie Gao [b,c,*], Yongfeng Wei [a], Hui Dou [a]

[a] Research and Development Center of Transport Industry of Technologies, Materials and Equipments of Highway Construction and Maintenance, (Gansu Road & Bridge Construction Group), Lanzhou 730030, Gansu, PR China
[b] Chang'an University, Xi'an 710064, PR China
[c] East China Jiaotong University, School of Transportation and Logistics, Nanchang 330013, PR China
[d] Sorbonne Université, Université de Technologie de Compiègne, CNRS, UMR 7253 Heudiasyc, CS 60319-60203 Compiègne Cedex, France

HIGHLIGHTS

- A study using GPR signals and NINs for pavement distress detection is presented.
- The NIN-based method detected pavement distresses with high precision.
- The NIN stability was not affected by GPR transmitting frequencies.
- The NIN-based method had a distinct superiority in detection effectiveness.

ARTICLE INFO

Article history:
Received 21 April 2019
Received in revised form 19 October 2019
Accepted 21 October 2019
Available online 31 October 2019

Keywords:
Pavement distress detection
Nondestructive testing
Network in network
Ground penetrating radar
Signal analysis

ABSTRACT

This study proposes a nondestructive testing technique for pavement distress detection using ground-penetrating radar and network in networks. Ground-penetrating radar signals are imported into two network-in-network structure as input data directly. The network in networks are used as deep learning models to distinguish abnormal signals, recognize distress types, and measure distress locations and sizes. A database with information from four highways is generated by a ground-penetrating radar with different transmitting frequencies and numbers of samples per trace. Then, the database is used to train, validate, and test the network in networks. The results show that the proposed method detects cracks, water-damage pits, and uneven settlements with 85.17% accuracy, 2.15 mm location errors, and reasonable stability. The proposed method was superior to other state-of-the-art techniques in terms of classification accuracy, location error, and stability. Additionally, the results show that this method overcomes the negative effect of transmitting frequencies in pavement distress detection using GPR data.

1. Introduction

Ground-penetrating radar (GPR) has been widely used as a nondestructive testing (NDT) technique for pavement distress detection and condition assessment [1,2]. A GPR system transmits electromagnetic waves with a specific frequency that can penetrate pavement structures. A portion of the waves is reflected when it hits underground pavement distresses such as cracks [3] or uneven settlements [4], the electromagnetic properties of which are different from those of the surrounding pavement materials. Then, the reflected waves are received by an antenna. Abnormal GPR signals such as hyperbolic-shaped signals from the reflected waves can be observed. These abnormal GPR signals are used to analyze pavement distress characteristics such as locations [5,6] and shapes [7,8].

Traditional pavement distress detection using GPR depends on four factors: (1) the frequency of an antenna signal; (2) velocity approximations of the transmitted and reflected electromagnetic waves; (3) the experience of an analyst in determining the abnormal values of the signals, such as the apex of the diffraction hyperbola; and (4) the decision rule how the type and intensity of the backscattered signal is a function of the shape and size of the anomalies. In practice, the frequency of a GPR antenna signal depends on the detection precision and depth. With the development of measurement technologies, the velocity approximations

* Corresponding author at: Chang'an University, Xi'an 710064, PR China.
** Co-corresponding author.
E-mail addresses: zheng.tong@hds.utc.fr (Z. Tong), highway-gaojie@st.chd.edu.cn (J. Gao).

https://doi.org/10.1016/j.conbuildmat.2019.117352
0950-0618/

of the transmitted and reflected electromagnetic waves can be calibrated with high precision based on the electromagnetic properties of the pavement materials in different layers of the structure [9]. However, an analyst may commit an error in determining the abnormal values of the GPR signals [10,11], not to mention the distress recognition. The rule selection for determining anomalous signals is also not solved well. In addition, noise data such as the data generated by the GPR vibration during inspection make the task more fallible [12,13]. Moreover, because many pavement distresses occur at one location, the analysis processes become more complex and challenging [14,15]. The challenge and significance of this issue have led researchers to develop many data processing techniques to partially replace the human inspection method.

Many signal processing techniques have been widely used as unsupervised methods to complete the task. For example, Qiao et al. [16] proposed a multi-step signal analysis method to detect buried objects, the location error of which was less than 5.8 cm. Li et al. [17] utilized the Hough transformation to identify objects with an accuracy of approximately 80%. Dou et al. [18] proposed a clustering method to separate the regions of interest from background signals. Liu et al. [19] used a short-time Fourier transform to identify the delamination between pavement layers. Rodés et al. [20] presented a possible analysis of the frequency spectrum of GPR signals for asphalt pavement assessment. Fernandes and Pais [21] used an amplitude-based signal processing technique to measure pavement crack widths. In addition, some coupling methods combining GPR and other NDT techniques were proposed to detect pavement distresses [22–24]. Although these methods show promising performances, they require expert operators who are familiar with both electromagnetic waves and pavement distresses. This means that these techniques cannot be widely used for pavement inspection. Additionally, the stability and transferability of these techniques are not desirable in practice. For example, certain signal processing techniques may offer high precision for some pavements but low precision for others.

Machine learning, as a supervised method, exhibits good object detection performance [25,26]. It has achieved remarkable success in pavement distress detection. There are two primary methods for pavement distress detection using GPR and machine learning: (1) Using received GPR signals to directly detect pavement distresses (e.g., Al-Nuaimy et al. [6] and Maas et al. [27] proposed neural network models to detect buried objects in pavements using GPR signals; Pasolli et al. [28] and Plati et al. [29] used genetic algorithms for object detection using GPR signals; Lu et al. [30] detected buried objects with high accuracy using a support vector machine and discrete wavelet transform.) However, these methods failed in some real-world conditions, such as multiple pavement layers and materials. This indicated that these methods were not stable in practice. Additionally, these methods only distinguished abnormal signals from normal ones but could not classify different buried objects and distresses.

(2) Using image-based detection. With the development of machine learning and GPR technology, GPR images began to be utilized to replace signals for pavement distress detection. For example, Tong and colleagues proposed deep-learning models to recognize, locate, and detect distresses using GPR images [31–33]. Sha et al. [34] utilized a cascade convolutional neural network to classify pavement distresses. All these studies showed that this direction for distress detection was influenced by the transmitting frequencies of GPR. Generally, the detection precision decreased drastically with decrement in the transmitting frequencies of GPR because of the signal to noise ratios and a capable interpreter for the data interpretation. In pavement inspection, some distresses reflect GPR signals with a high signal to noise ratio, thereby complicating data interpretation for these signals. Additionally, some noises are easily determined as distresses [31].

Motived by the shortcomings of the previous studies [31–33], we reconsidered the possibility of combining GPR signals and state-of-the-art deep-learning models to detect pavement distresses. Therefore, this paper presents an innovative attempt to use GPR signals and network in networks (NINs) to detect pavement distresses. The contributions and advantages of this study are summarized below:

(1) The proposed method detected pavement distresses (e.g., crack, water-damage pit, uneven settlement) with high precision. Its stability was not affected by pavement structures and GPR transmitting frequencies. It overcame the disadvantages of the previous studies [31–33].
(2) Many state-of-the-art techniques in deep learning (e.g., target dropout, global average pooling, and layer-sequential unit-variance initialization) were adopted to remarkably improve the accuracy of the proposed model.
(3) With the assistance of the proposed method, the processes of pavement distress detection did not require experience of an analyst specializing in electromagnetic waves and deep learning; while the proposed model played the role of an inspector with long-term experience and a good theoretical knowledge.

The rest of this paper is organized as follows. In Section 2, we present the experimental details regarding GPR signal collection and the selection of tested road sections and GPR equipment parameters. In Section 3, we introduce the NIN-based method for distress detection, including abnormal-signal recognition, pavement-distress classification and measurement, and implementation details. In Section 4, we discuss the performance of the NIN-based method. Finally, Section 4 summarizes the conclusions.

2. Experimental details

2.1. Tested road sections

The tested road sections were in the Heilongjiang province in China, as shown in Fig. 1. GPR inspection was conducted on four highways that were made of asphalt pavements, and had a total length of 27,820 m. The four highways had different service lives, structures, and materials to ensure the integrity of the GPR database.

2.2. GPR equipment and measurement method

An OKO-2 GPR system was used in this study. Because the expected detection depths were approximately 0.3–0.6 m, referring to the study of Annan [35], only the data in the first ten ns time windows were used in this study. Three transmitting frequencies (300, 600, and 900 MHz) and numbers of samples per trace (256, 384, and 512) were adopted for scanning the four highways to guarantee the integrity of the GPR database. The vertical resolution ranges of the three transmitting frequencies were 0.003–0.005 m, 0.002–0.003 m, and 0.001–0.002 m, whereas the horizontal resolutions were 0.08–0.1 m, 0.05–0.06 m, 0.04–0.05 m, respectively. The trace-interval distance in this study was 0.015 m. Considering that the widths of the cracks and other distresses were generally larger than 0.015 m, the trace-interval distance and horizontal resolutions were acceptable.

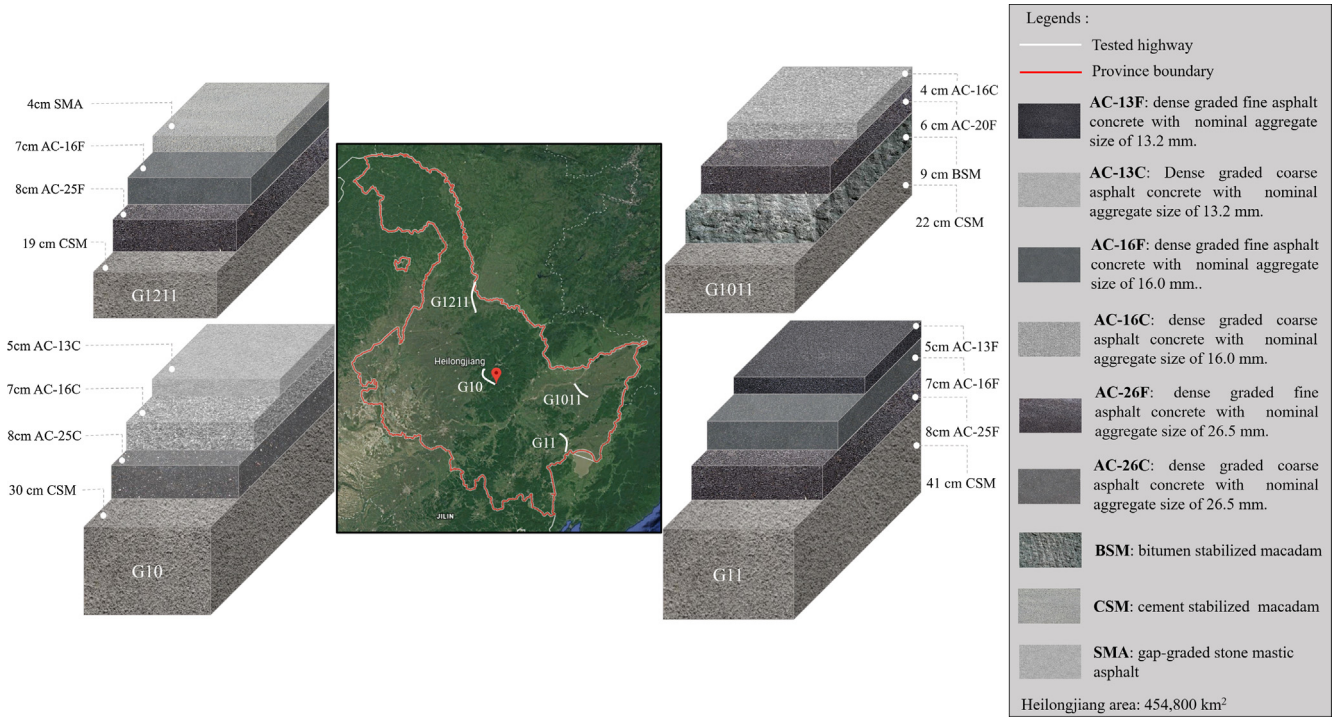

Fig. 1. Distribution, constructions, and materials of tested roads. The map is acquired from Google Earth.

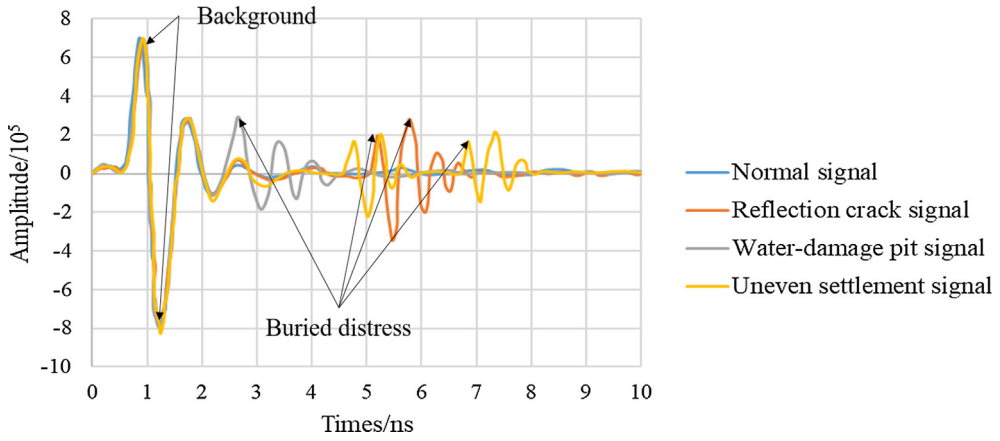

Fig. 2. Typical GPR signals in 600 MHz (A-scanning).

Fig. 2 presents normal and abnormal GPR signals from a crack, a water-damage pit, and an uneven settlement. The characteristics of abnormal signals are different from those of normal signals. However, two tasks need to be accomplished: (1) Determining a way to differentiate a normal GPR signal from an abnormal GPR signal—the characteristics of abnormal GPR signals vary from one distress to another, and it is difficult for analysts to describe them formally; (2) Using these abnormal GPR signals to recognize and measure pavement distresses.

Fig. 3 presents GPR images using B-scanning. The distress types that are shown in Fig. 3 were determined by core sampling. As shown in Fig. 3, the feature of each anomalous signal can be related to a specific type of pavement distresses. This indicates that a set of GPR signals can be used to detect pavement distresses. Two steps were designed to detect pavement distresses using GPR signals and NINs. First, a NIN was designed to differentiate a normal GPR signal from abnormal ones. Next, another NIN was utilized to classify and measure the set of abnormal GPR signals.

3. Algorithm for distress detection

In this section, we introduce the NIN model for recognizing abnormal GPR signals in Section 3.1. Then, we describe the NIN for classifying and measuring different pavement distresses based on the abnormal signals in Section 3.2. Finally, Section 3.3 presents implementation details and the database for the study.

3.1. Recognition of abnormal GPR signals

The first step in detecting pavement distresses using GPR signals is to recognize abnormal signals in received electromagnetic waves. The multilayer perceptron [26,27] has been reported to conduct abnormal signal recognition based on the provided features. However, it failed to classify different GPR signals owing to its shallow structure. From the deep learning perspective, an algorithm can be considered as a deep one if it can extract low-level

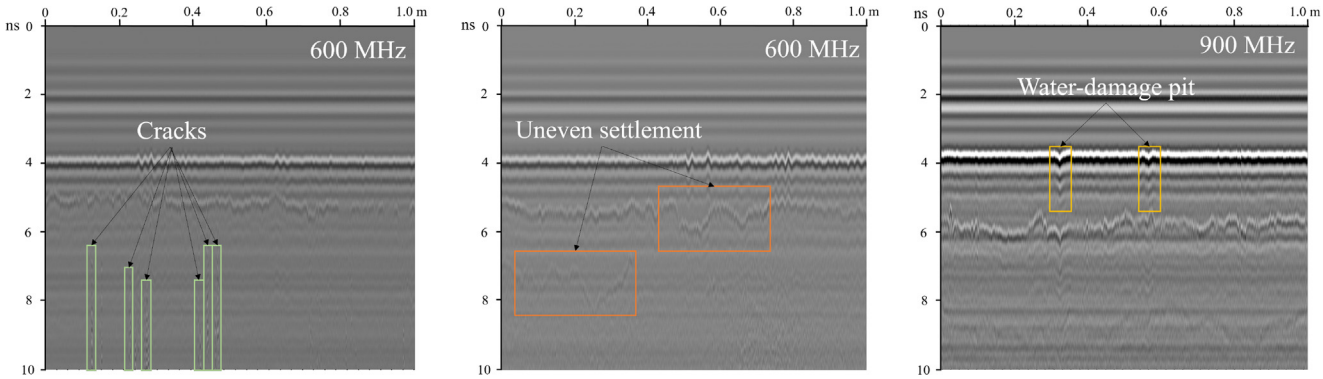

Fig. 3. Typical GPR images (B-scanning).

features related to the class membership from raw data and integrate them into high-level features for a classification task [36]. However, a multilayer perceptron requires features to be provided by an analyst. Thus, the structure of a multilayer perceptron is shallow. In this study, multilayer perceptrons deepened themselves in a convolutional-neural-network mode to extract low-level features and integrate them into high-level features autonomously, as shown in Fig. 4 and Table 1. This model were called network in network (NIN) and its special layers are called multilayer perceptron (MLP) layers. Notably, the NIN can be considered as a deep-learning model because it learned multiple-level features [36]. Fig. 4 indicates that there are two special layers in the NIN:

(1) MLP layer—A Multilayer perceptron with two layers was used to convolve over the input data in an MLP layer. Each multilayer perceptron was considered as a nonlinear filter to extract certain features from the input data as

$$\begin{aligned} f_{i,k_1}^{1} &= \max\left(\left(w_{k_1}^{1}\right)^{T} x_i + b_{k_1}, 0\right) \\ &\vdots \\ f_{i,k_1}^{n} &= \max\left(\left(w_{k_n}^{n}\right)^{T} f_{i,k_1}^{n-1} + b_{k_n}, 0\right) \end{aligned}, \quad (1)$$

where n is the number of layers in the NIN; i is the number of input-data points; w_{kn}^{n} and b_{kn} are the weights and bias in the n^{th} layer, respectively. With n multilayer perceptrons in different MLP layers, we could acquire various low-, medium-, and high-level features related to abnormal signals from real-world GPR data. The function of an MLP layer is similar to that of a convolutional layer in a deep-learning model, but it performs better.

Compared with traditional deep-learning models, there is no pooling layer following the MLP layer in the NIN because pooling layers were replaced by MLP layers with an increased stride as shown in Table 1. The replacement led to an improvement in accuracy that was verified in the study conducted by Springenberg [37].

(2) Global average pooling layer—A traditional deep-learning model vectorizes the features from the last convolutional layer and feeds it into fully connected layers (FCNs) for classification [38,39]. However, FCNs may lead to overfitting and hamper the generalization of the network [39] even with a target dropout [40]. Referring to the study conducted by Lin et al. [41], a global average pooling (GAP) layer was utilized to replace the FCNs. Instead of vectorizing features in the FCNs, a GAP layer took the average of the features and fed the results into a softmax layer for abnormal signal recognition.

3.2. Detection for pavement distresses

The second step in detecting pavement distress detection is to classify and measure the distresses. Considering the sizes and orientations of different pavement distresses as presented in Table 2, GPR signals in a 1-meter pavement were imported into a NIN for detecting pavement distresses. Fig. 5 and Table 3 present the details of the NIN. The NIN used for this step had a similar structure to the NIN for the first step except for the input and output layers.

(1) In the input layer, GPR signals were labeled as "0" or "1" on the basis of the outputs of the NIN for recognizing abnormal signals. In the study, "0" and "1" represent as "abnormal signal" and "normal signal", respectively. Then the GPR signals and labels were imported into the second-step NIN.
(2) In the output layers, we designed a softmax layer for classification and three regression layers for measurement. As shown in Fig. 5, the GPR signals and labels passed through the MLP layers and a GAP layer in sequence. Then, the averaged features were first imported into a softmax layer, wherein a multi-class output was generated. Once the output indicated that there was at least one type of pavement distress, the averaged features were imported into one or more regression layers for distress measurement. For exam-

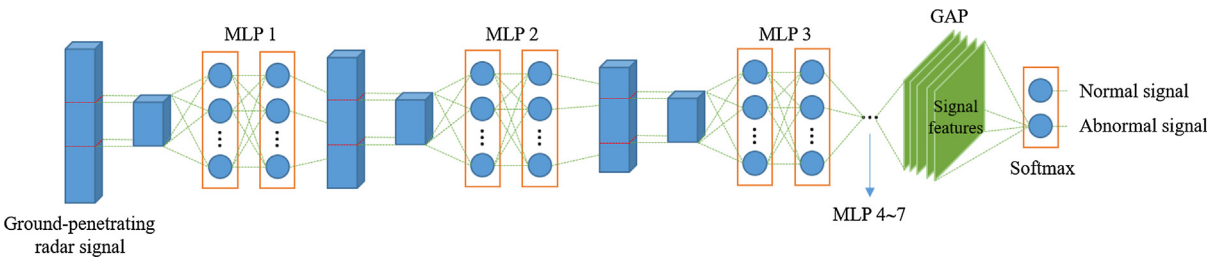

Fig. 4. Overall structure of network in network to recognize abnormal GPR signals. MLP and GAP are multilayer perceptron and global average pooling, respectively.

Table 1
Parameters of network in network to recognize abnormal GPR signals.

Layer number	Layer type	Input size	Multilayer perceptron size				Stride
			Input	Layer 1	Layer 2	Output	
L1	Input	128 × 1	–	–	–	–	–
L2	MLP 1	128 × 1	10 × 1	10	10	10 × 48	1
L3	MLP 2	119 × 1	10 × 1	10	10	10 × 48	1
L4	MLP 3	110 × 1	10 × 1	10	10	10 × 48	2
L5	MLP 4	50 × 1	8 × 1	7	7	8 × 96	1
L6	MLP 5	43 × 1	8 × 1	7	7	8 × 96	1
L7	MLP 6	36 × 1	8 × 1	7	7	8 × 96	2
L8	MLP 7	14 × 1	6 × 1	7	7	6 × 192	1
L9	MLP 8	9 × 1	6 × 1	7	7	6 × 192	1
L10	MLP 9	4 × 1	4 × 1	7	7	4 × 192	1
L11	GAP	4 × 192	–	–	–	–	1
L12	Softmax	2 × 1	–	–	–	–	1

Table 2
Overall distributions and sizes of different pavement distresses.

Type	Orientation	Size/m	Depth/m
Crack	Direction or vertical direction of highways	(0.01–0.03) × (0.10–1.00)	0.01–0.60
Water-damage pit	Direction and vertical direction of highways	(0.05–0.30) × (0.05–0.30)	0.15–0.60
Uneven settlement	Direction of highways	(0.05–1.00) × (0.05–1.00)	0–0.05

ple, the global features were imported into a crack regression layer if the output of the softmax layer indicated that the GPR signals suggest a crack in the 1-meter pavement. The features were imported into two or three regression layers if the GPR signals reflected two or three different distresses in the 1-meter pavement. Notably, the outputs of the three regression layers are different, as shown in Fig. 5. The distress detection was conducted based on the outputs of the softmax layer and three regression layers.

3.3. Implementation details and database

Four highways with a total length of 27,820 m were inspected using GPR as introduced in Section 2. To verify the stability of the NIN-based method, we scanned the 27,820 m pavements using three transmitting frequencies (300, 500, 900 MHz) and numbers of sample per trace (128, 256, and 384). Both data ratios of the three transmitting frequencies and numbers of sample per trace were 1:1:1. We annotated two types of labels for the database. The first type labels was annotated for each GPR signal to state whether the signal is normal or not and was used to train the NIN to recognize abnormal GPR signals. The second type of labels was annotated for each GPR data in a 1-meter pavement to state whether there was a distress or not and the location information of each distress, which were used to train the NIN to locate pavement distresses. Notably, the distress types in the database were determined by core sampling. We selected 16,692 and 5564 1-meter lengths of GPR data randomly from the database as a training and validation data set, respectively. The remaining 5564 1-meter lengths of GPR data were used as a testing data set. We used 1500 GPR signals and 500 m GPR data for the two NINs in each epoch.

Additionally, a stochastic gradient descent [42] and layer-sequential unit-variance initialization (LSUV) [43] were adopted in this study to further improve the precision of the two NINs. The LSUV was used to provide initialized weights for the two NINs, whereas the stochastic gradient descent was used for training the two NINs.

The processes in Section 3 were conducted in a Python environment with a computer with a Core i7 8750H @ 3.4 GHz CPU, 32 GB of DDR4 memory, and an 8 GB NVIDIA 1080 GPU.

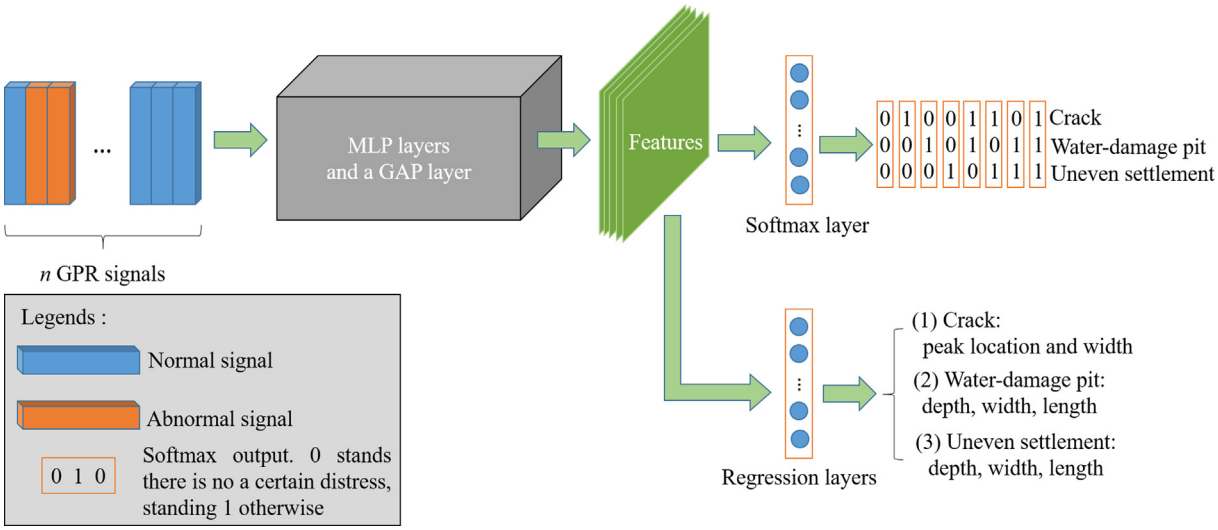

Fig. 5. Overall structure of network in network to detect pavement distresses. MLP and GAP are multilayer perceptron and global average pooling, respectively.

Table 3
Parameters of network in network to detect pavement distresses.

Layer number	Layer type	Input size	Multilayer perceptron size				Stride
			Input	Layer 1	Layer 2	Output	
L1	Input	$128 \times n$	–	–	–	–	–
L2	MLP 1	$128 \times n$	10×1	10	10	10×48	1
L3	MLP 2	119×1	10×1	10	10	10×48	1
L4	MLP 3	110×1	10×1	10	10	10×48	2
L5	MLP 4	50×1	8×1	7	7	8×96	1
L6	MLP 5	43×1	8×1	7	7	8×96	1
L7	MLP 6	36×1	8×1	7	7	8×96	2
L8	MLP 7	14×1	6×1	7	7	6×192	1
L9	MLP 8	9×1	6×1	7	7	6×192	1
L10	MLP 9	4×1	4×1	7	7	4×192	1
L11	GAP	4×192	–	–	–	–	1
L12	Softmax	8×1	–	–	–	–	1
L13	Regression	m	–	–	–	–	1

Note: n is the GPR signal number in a 1 m pavement, which depends on the distance of the transmitter–receiver positions. m is the number of measurement results relating to different pavement distresses, which depends on the distress types.

4. Results and discussion

4.1. Recognition performance

4.1.1. Overall performance

Fig. 6 presents the training, validation, and testing accuracies of the NIN for recognizing abnormal GPR signals. After the 1000th epoch, the accuracies of training, validation, and testing were 97.52%, 95.67%, and 95.94%, respectively. Additionally, the accuracies were stable between the 1000th and 1500th epochs. The accuracy fluctuations between the 1000th and 1500th epochs indicated that the recognition performance of the NIN was reasonable after the 1000th epoch. The gap between the validation and testing accuracies verified that the NIN precisely distinguished abnormal GPR signals from normal ones. This showed that the NIN had an acceptable generalization ability for abnormal GPR signal recognition.

4.1.2. Stability analysis

Two stability analyses were conducted to verify the robustness of the NIN, including transmitting frequencies (300, 600, and 900 MHz) and pavement structures (G10, G1011, G11, G1211). The testing data set was divided into different parts based on the types of GPR data, such as different transmitting frequencies. The NIN was used to recognize abnormal GPR signals in these different parts.

Fig. 7 presents the confusion matrices of the two stability analyses. Notably, only the testing results were reported in Fig. 7. Fig. 7 (a) showed that the accuracies of the abnormal signal recognition for different transmitting frequencies were close. This indicated that the performance of the NIN was not evidently influenced by the transmitting frequencies. It also verified that the NIN provided useful abnormal-signal labels for the distress detection in the second step when the transmitting frequency for GPR antenna was higher than 300 MHz. The lowest transmitting frequency could meet the demands of the pavement inspection. Fig. 7(b) showed that the performance of the NIN in different pavement structures and materials was similar. This indicated that the pavement structures did not influence the performance of the NIN.

Fig. 8 presents the error distribution for different depths of abnormal signal points. The error distribution was uniform for different depths. This indicated that the depth of the distress had a limited effect on the abnormal signal recognition. However, considering the horizontal resolutions in the three transmitting frequencies, the accuracy was affected by the sizes of the distresses. For example, it was difficult for the GPR and the proposed model to recognize cracks whose widths were less than 0.001 m. Therefore, the NIN accuracy may be further improved by utilizing trans-

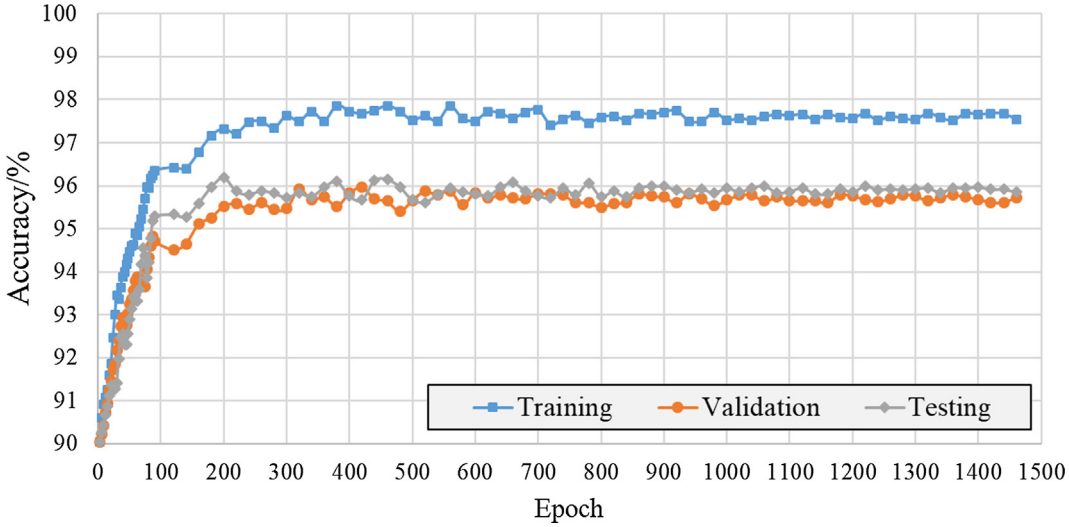

Fig. 6. Training, validation, and testing accuracy of the recognition NIN.

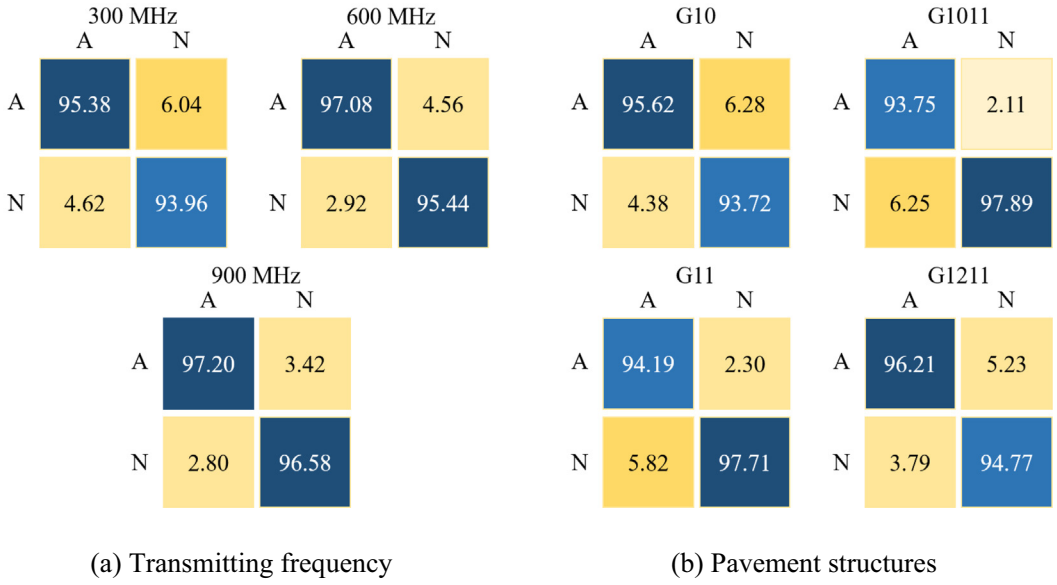

Fig. 7. Confusion matrixes of stability analyses for the recognition NIN (Unit: %). "A" and "N" stand abnormal and normal signals, respectively.

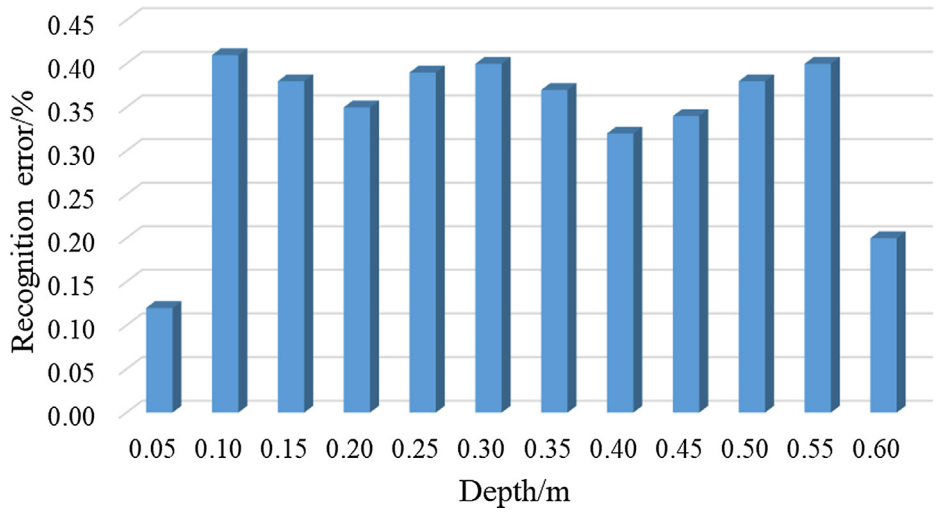

Fig. 8. Error distribution vs depths of abnormal signal points.

mitting frequencies with higher resolutions. However, the increase of signal frequencies does not always result in a better ability to detect a crack because an anomalous signal is often given by diffraction hyperboles, which is created when the size of the object is smaller than the wavelength of the GPR signal.

4.2. Classification performance

4.2.1. Overall performance

Compared with the NIN for abnormal signal recognition, there were two aims for the NIN for distress detection. The first one was to classify distress classes using GPR signals from a 1-meter pavement. The average accuracy was used to evaluate the NIN performance for this purpose. The second one was to locate the distresses in a 1-meter pavement, as shown in Fig. 5. The average loss, shown in Eq. (2), was used to evaluate the performance of the NIN for this purpose as

$$Average\_loss = \sqrt{\frac{1}{n \cdot m \cdot l} \sum_{i=1}^{n} \sum_{j=1}^{m} \sum_{k=1}^{l} \left(x_{ijk} - x'_{ijk} \right)^2} \quad (2)$$

where i is the number of the GPR data in an epoch; j is the number of characteristics of a certain distress as shown in Fig. 5; and l is the number of distresses in the GPR data. $xijk$ and $x'ijk$ are the true value and the predicted value by the NIN.

Fig. 9 presents the training, validation, and testing accuracies and losses of the NIN for detecting pavement distresses. After 12,000 iterations, the accuracies for training, validation, and testing were 89.02%, 86.49%, and 85.17%, while the losses were 1.86 mm, 2.08 mm, and 2.15 mm, respectively. The classification accuracies and location errors met the demands of pavement inspection [44]. The losses were close to the GPR resolution. This indicated that the NIN errors were not the primary factors influencing the precision of the distress measurements, but the GPR errors were. Additionally, the accuracies and losses were stable between the 10000th and 12000th epochs. The accuracy and loss fluctuations between the 10000th and 12000th epochs indicated that the detection performance of the NIN was reasonable after 10,000 epochs. The gap between the validation and testing results verified that the NIN could classify and measure different distresses. This showed that the NIN had an acceptable generalization

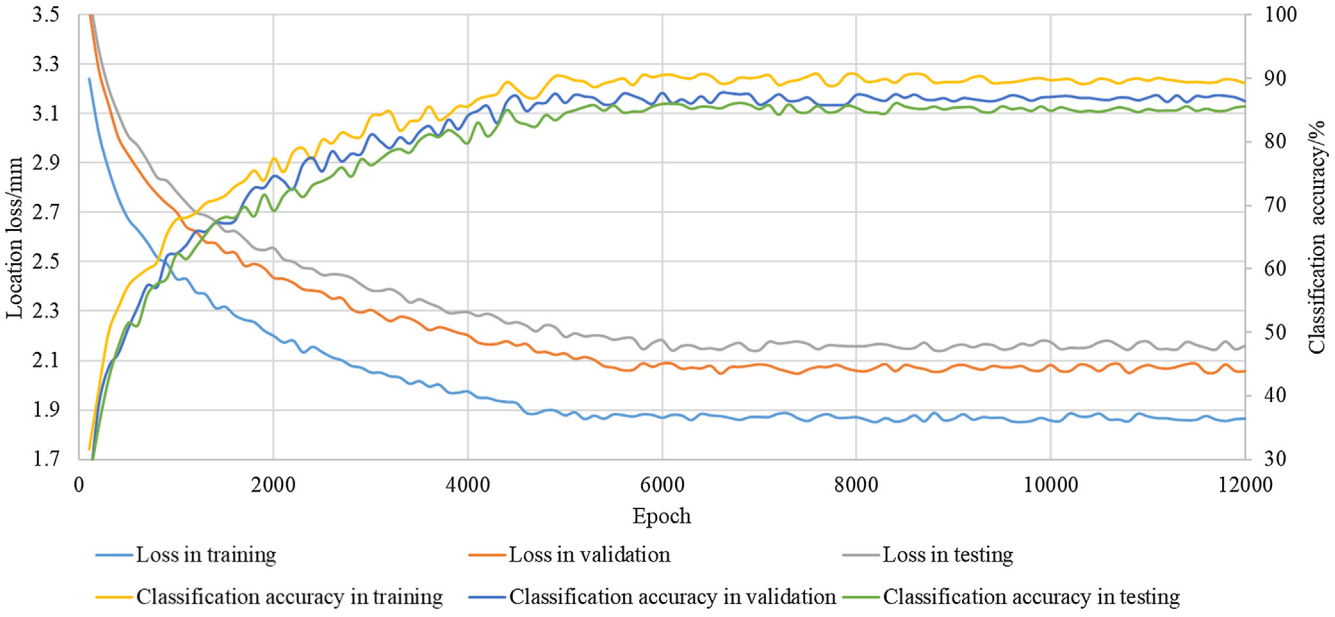

Fig. 9. Training, validation, and testing accuracy of the detection NIN.

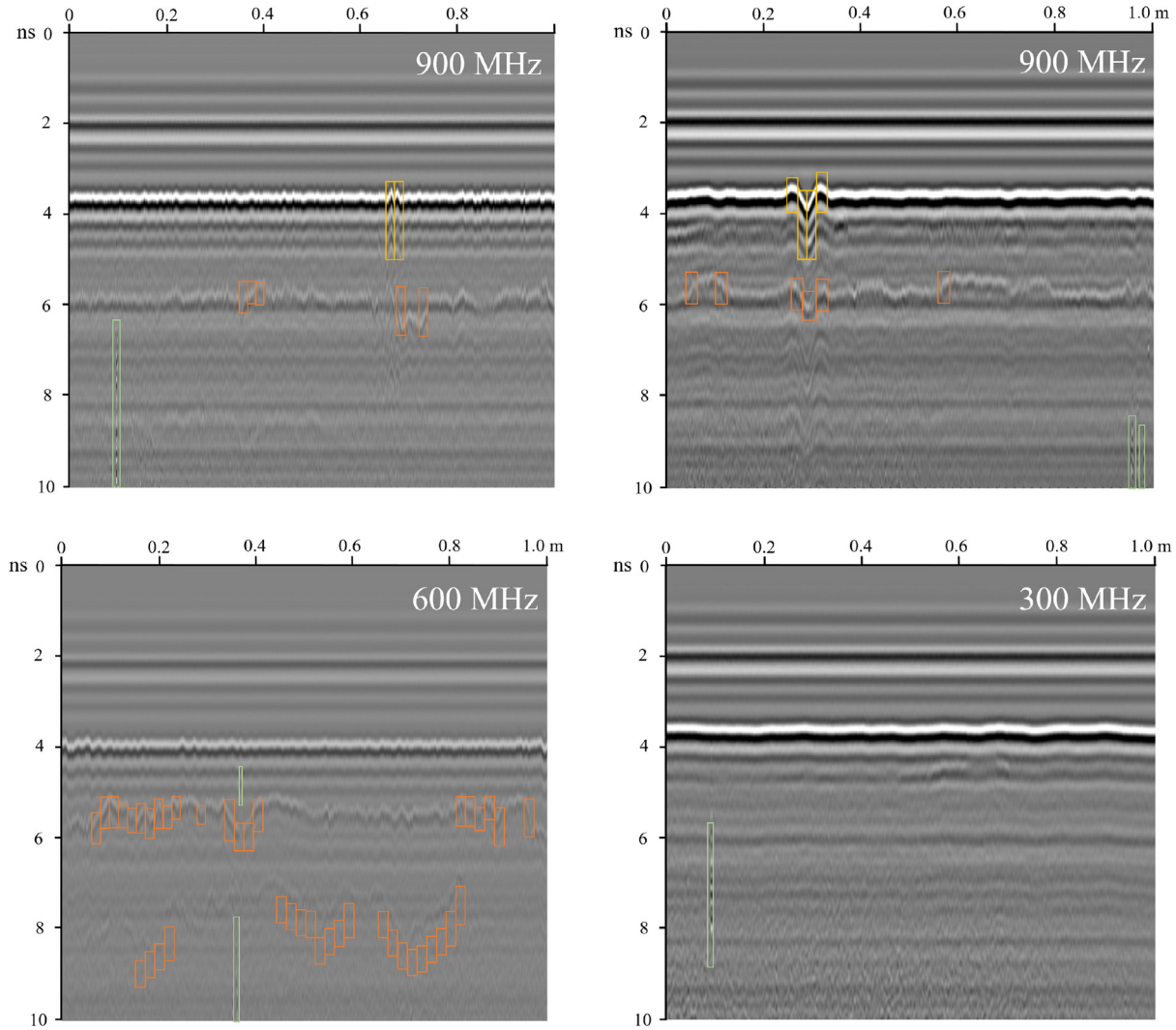

Fig. 10. Examples of pavement distress detection. The distresses in green, yellow, and orange boxes are cracks, water-damage pits, and uneven settlement. (For interpretation of the references to colour in this figure legend, the reader is referred to the web version of this article.)

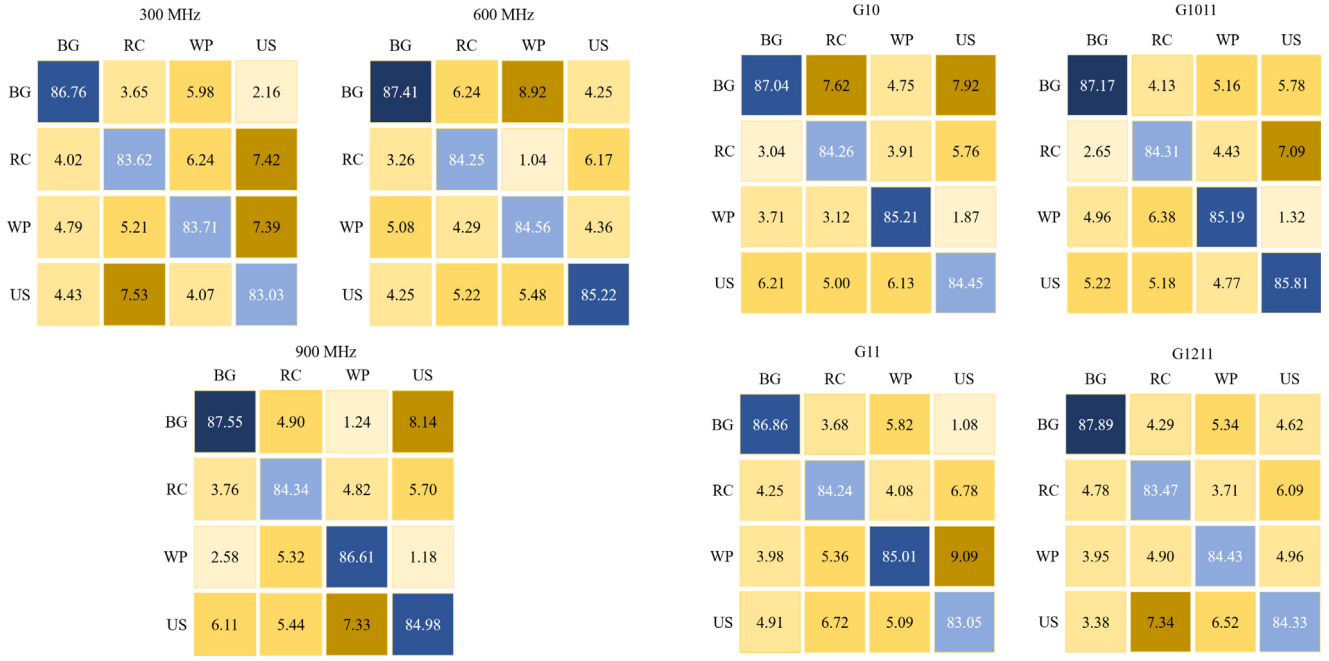

(a) Transmitting frequency

(b) Pavement structures

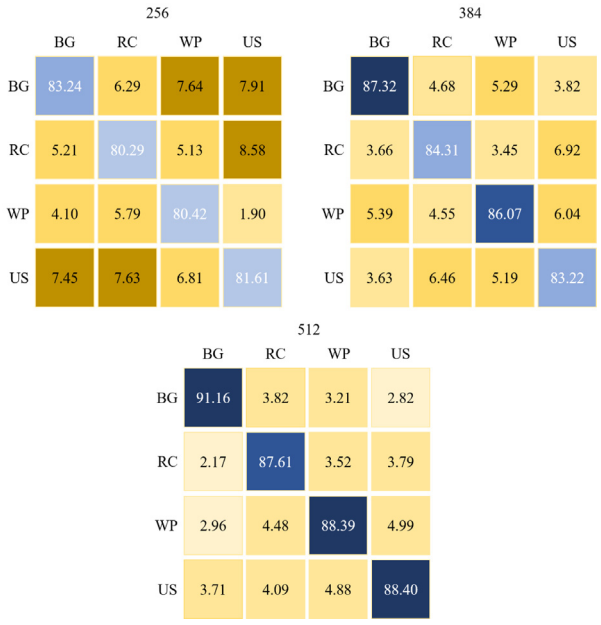

(c) Numbers of samples per trace

Fig. 11. Confusion matrixes of stability analyses for the detection NIN. BG, RC, WP, US are background, crack, water-damage pit, and uneven settlement, respectively.

Table 4
Losses of the NIN for pavement distress detection (Unit: mm).

	Transmitting frequency/MHz			Sweep sampling number/Hz			Pavement structures			
	300	600	900	256	384	512	G10	G1011	G11	G1211
Loss	2.26	2.17	2.02	2.54	2.08	1.83	2.18	2.09	2.20	2.13

Table 5
Average accuracies and losses in a comparative study.

Factors		NIN		Faster R-CNN		GA and SVM	
		Accuracy	Loss	Accuracy	Loss	Accuracy	Loss
Transmitting frequency/MHz	300	84.28	2.26	78.90	4.07	67.25	11.43
	600	85.36	2.17	81.42	3.52	74.82	10.42
	900	85.87	2.02	83.43	2.13	76.21	10.10
Pavement structure	G10	85.24	2.54	81.08	3.47	73.26	10.35
	G1011	85.62	2.08	81.37	3.19	71.05	10.91
	G11	84.79	1.83	81.25	3.31	72.63	10.37
	G1211	85.03	2.18	81.30	2.99	74.10	10.97
Sweep sampling number/Hz	256	81.39	2.09	77.24	4.51	66.28	11.59
	384	85.23	2.20	82.19	3.10	75.02	10.24
	512	88.89	2.13	84.32	2.11	76.98	10.21

Note: Units of accuracy and loss are % and mm.

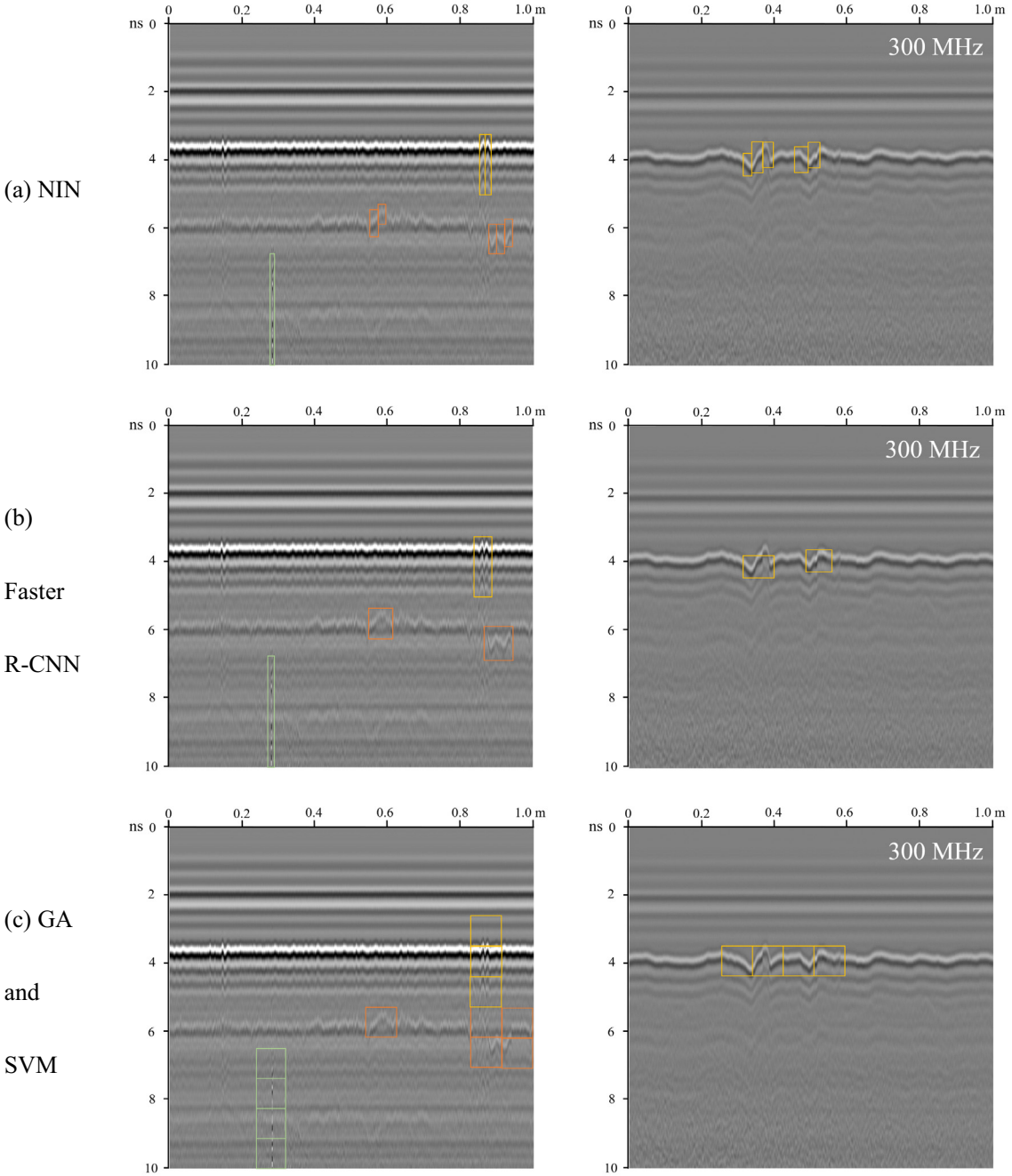

Fig. 12. Examples of a comparative study. The distresses in green, yellow, and orange boxes are cracks, water-damage pits, and uneven settlement, respectively. (For interpretation of the references to colour in this figure legend, the reader is referred to the web version of this article.)

ability for distress detection in general. Some of the detection results are shown in Fig. 10. In Fig. 10, cracks, water-damage pits, and uneven settlement were precisely detected by the NIN.

4.2.2. Stability analysis

Three stability analyses were conducted to verify the robustness of the NIN, including transmitting frequencies (300, 600, and 900 MHz), numbers of samples per trace (256, 384, and 512 Hz), and pavement structures (G10, G1011, G11, and G1211). The testing data set was divided into different parts based on the types of GPR data, such as different transmitting frequencies. The NIN was used to detect pavement distresses in these different parts.

Fig. 11 presents the confusion matrixes of the three-stability analyses for classification accuracies. Only the testing results are reported in Fig. 11. Fig. 11(a) shows that the accuracies of distress recognition in different transmitting frequencies were close. This indicated that the NIN performance was not influenced by the transmitting frequencies when the transmitting frequencies of the GPR antenna were higher than 300 MHz. Considering the penetrability of the 300 MHz electromagnetic waves in asphalt pavements, the lowest transmitting frequencies in this study met the demands of the pavement inspection [36]. Fig. 11(b) shows that the NIN performances in different pavement structures and materials were similar. This indicated that the pavements did not influence the performance of the NIN. However, Fig. 11(c) shows that the classification accuracies varied for different numbers of samples per trace. This was because the GPR acquired more signals in 1-meter pavements with the increment in the numbers of samples per trace. One-meter GPR data with a higher number of signals provided more information about pavement distresses for the NIN. However, Fig. 11(c) demonstrates that even the classification accuracy of the lowest number of samples per trace in the study was still reasonable for pavement inspection. Thus, the number of samples per trace did not influence the accuracy of the method if that number was greater higher than 256.

Table 4 presents the losses of the three-stability analyses for the distress location. The losses in the NIN were not influenced by the pavement structures and transmitting frequencies, but they were affected by the number of samples per trace. However, even the loss with the lowest number of samples per trace was still reasonable for pavement inspection [36].

4.3. Comparative study

The NIN-based method was compared with state-of-the-art methods to verify its effectiveness. Because the disadvantages of unsupervised algorithms for distress detection using GPR data have been verified in previous studies [24], two supervised algorithms were selected in this study. The first one [26] was a method using a faster regional convolutional network (Faster R-CNN) and GPR images, while the second one [22] was based on GA and SVM using GPR signals.

Table 5 presents the average accuracies and losses of the three methods. Fig. 12 presents some results of the comparative study. The results showed that the precision and stability of the NIN-based method were optimal, which produced a high accuracy and low loss in various real-world conditions, including different transmitting frequencies, numbers of samples per trace, and pavement structures. However, the accuracy and loss of the Faster R-CNN were unstable in different transmitting frequencies and numbers of samples per trace, which was the same was reported in our previous study [26]. This was because the GPR images were easily affected by the resolutions and noise ratios of the GPR equipment. Unfortunately, the accuracy and loss of the method based on GA and SVM were unreasonable in real-world conditions. Therefore, the comparative study showed that the NIN-based method was superior in pavement distress detection using GPR signals.

5. Conclusions

A study using GPR signals and NINs for pavement detection is presented in this paper, and the following conclusions can be drawn:

(1) The NIN-based method detected pavement distresses such as cracks, water-damage pits, and uneven settlements with 85.17% precision and 2.15 mm location errors in real-world conditions for different pavement structures and materials, transmitting frequencies, and number of samples per trace. Thus, the proposed method can be regarded as an autonomous NDT method.
(2) The NIN for abnormal GPR signal recognition achieved an average accuracy of 95.94% in the testing. The accuracy of the NIN was not influenced by transmitting frequencies and pavement structures. The distress depths had a limited effect on the abnormal signal recognition, whereas the NIN accuracy was affected by the sizes of the distresses because of the resolutions of different transmitting frequencies. Thus, the NIN accuracy may be further improved by utilizing transmitting frequencies with higher resolutions.
(3) The NIN for distress recognition and location achieved an 85.17% average classification accuracy and 2.15 mm location errors in the testing. The accuracy of the NIN was not influenced by transmitting frequencies, pavement structures, and the distress depths. Thus, the NIN can recognize and locate pavement distresses using GPR signals in real-world conditions.
(4) The comparative study showed that the NIN-based method had a distinct superiority in the effectiveness of distress recognition, location, and measurement. Additionally, the study showed that this method overcame the negative influence of low transmitting frequencies in pavement distress detection to some degree.
(5) A more advanced deep-learning model must be developed to improve the stability of the proposed method for different cases of number of samples per trace using GPR signals, and this will be the focus of our future research.

Declaration of Competing Interest

The authors declare that they have no known competing financial interests or personal relationships that could have appeared to influence the work reported in this paper.

Acknowledgements

The authors gratefully acknowledge the financial support provided by Opening Foundation of Research and Development Center of Transport Industry of Technologies, Materials and Equipments of Highway Construction and Maintenance (Gansu Road & Bridge Construction Group) (No. GLKF201811). This work is also supported by Co-operation Program with the UTs and INSAs (France) funded by the China Scholarship Council (No. CSC201801810108).

References

[1] D.J. Daniels. Ground penetrating radar. Encyclopedia of RF and Microwave Engineering, (2005).
[2] A. Benedetto, L. Pajewski (Eds.), Civil Engineering Applications of Ground Penetrating Radar, Springer, 2015.

[3] Q. Lu, J. Pu, Z. Liu, Feature extraction and automatic material classification of underground objects from ground penetrating radar data, J. Electric. Comput. Eng. 2014 (2014) 28.
[4] X. Xu, J. Wu, J. Shen, Z. He, Case study: application of GPR to detection of hidden dangers to underwater hydraulic structures, J. Hydraulic Eng. 132 (1) (2006) 12–20.
[5] S. Jazayeri, A. Saghafi, S. Esmaeili, C.P. Tsokos, Automatic object detection using dynamic time warping on ground penetrating radar signals, Expert Syst. Appl. 122 (2019) 102–107.
[6] W. Al-Nuaimy, Y. Huang, M. Nakhkash, M.T.C. Fang, V.T. Nguyen, A. Eriksen, Automatic detection of buried utilities and solid objects with GPR using neural networks and pattern recognition, J. Appl. Geophys. 43 (2–4) (2000) 157–165.
[7] S. Jazayeri, A. Klotzsche, S. Kruse, Improving estimates of buried pipe diameter and infilling material from ground-penetrating radar profiles with full-waveform inversion, Geophysics 83 (4) (2018) H27–H41.
[8] A.K. Khamzin, A.V. Varnavina, E.V. Torgashov, N.L. Anderson, L.H. Sneed, Utilization of air-launched ground penetrating radar (GPR) for pavement condition assessment, Constr. Build. Mater. 141 (2017) 130–139.
[9] J.F. Sham, W.W. Lai, Development of a new algorithm for accurate estimation of GPR's wave propagation velocity by common-offset survey method, NDT E Int. 83 (2016) 104–113.
[10] X. Xu, Q. Zeng, D. Li, J. Wu, X. Wu, J. Shen, GPR detection of several common subsurface voids inside dikes and dams, Eng. Geol. 111 (1–4) (2010) 31–42.
[11] S. Zhao, I.L. Al-Qadi, Development of an analytic approach utilizing the extended common midpoint method to estimate asphalt pavement thickness with 3-D ground-penetrating radar, NDT E Int. 78 (2016) 29–36.
[12] H. ShuangGui, T. JingTian, R. ZhengYong, Z. Cong, X. Xiao, Normalized facet edge detection and enhancement in potential field sources with the scale-space technique, Chin. J. Geophys.-Chin. Ed. 62 (1) (2019) 331–342.
[13] D. Xiang, K. Zhou, Y. Su, Fast prescreening for GPR antipersonnel mine detection via go decomposition, IEEE Geosci. Remote Sens. Lett. 16 (1) (2018) 15–19.
[14] Y. Pan, X. Zhang, G. Cervone, L. Yang, Detection of asphalt pavement potholes and cracks based on the unmanned aerial vehicle multispectral imagery, IEEE J. Sel. Top. Appl. Earth Obs. Remote Sens. 11 (10) (2018) 3701–3712.
[15] L. Yi, L. Zou, K. Takahashi, M. Sato, High-resolution velocity analysis method using the ℓ-1 norm regularized least-squares method for pavement inspection, IEEE J. Sel. Top. Appl. Earth Obs. Remote Sens. 11 (3) (2018) 1005–1015.
[16] L. Qiao, Y. Qin, X. Ren, Q. Wang, Identification of buried objects in GPR using amplitude modulated signals extracted from multiresolution monogenic signal analysis, Sensors 15 (12) (2015) 30340–30350.
[17] W. Li, X. Cui, L. Guo, J. Chen, X. Chen, X. Cao, Tree root automatic recognition in ground penetrating radar profiles based on randomized Hough transform, Remote Sens. 8 (5) (2016) 430.
[18] Q. Dou, L. Wei, D.R. Magee, A.G. Cohn, Real-time hyperbola recognition and fitting in GPR data, IEEE Trans. Geosci. Remote Sens. 55 (1) (2016) 51–62.
[19] H. Liu, Z. Deng, F. Han, Y. Xia, Q.H. Liu, M. Sato, Time-frequency analysis of air-coupled GPR data for identification of delamination between pavement layers, Constr. Build. Mater. 154 (2017) 1207–1215.
[20] J.P. Rodés, V. Pérez-Gracia, A. Martínez-Reguero, Evaluation of the GPR frequency spectra in asphalt pavement assessment, Constr. Build. Mater. 96 (2015) 181–188.
[21] F.M. Fernandes, J.C. Pais, Laboratory observation of cracks in road pavements with GPR, Constr. Build. Mater. 154 (2017) 1130–1138.
[22] V. Marecos, M. Solla, S. Fontul, V. Antunes, Assessing the pavement subgrade by combining different non-destructive methods, Constr. Build. Mater. 135 (2017) 76–85.
[23] S. Lagüela, M. Solla, I. Puente, F.J. Prego, Joint use of GPR, IRT and TLS techniques for the integral damage detection in paving, Constr. Build. Mater. 174 (2018) 749–760.
[24] A.H. Alavi, H. Hasni, N. Lajnef, K. Chatti, Continuous health monitoring of pavement systems using smart sensing technology, Constr. Build. Mater. 114 (2016) 719–736.
[25] Y. LeCun, Y. Bengio, G. Hinton, Deep learning, Nature 521 (7553) (2015) 436.
[26] Z. Tong, J. Gao, A. Sha, L. Hu, S. Li, Convolutional neural network for asphalt pavement surface texture analysis, Comput.-Aided Civ. Infrastruct. Eng. 33 (12) (2018) 1056–1072.
[27] C. Maas, J. Schmalzl, Using pattern recognition to automatically localize reflection hyperbolas in data from ground penetrating radar, Comput. Geosci. 58 (2013) 116–125.
[28] E. Pasolli, F. Melgani, M. Donelli, R. Attoui, M. De Vos, Automatic detection and classification of buried objects in GPR images using genetic algorithms and support vector machines pp. II-525, IGARSS 2008-2008 IEEE International Geoscience and Remote Sensing Symposium, IEEE, 2008.
[29] C. Plati, K. Georgouli, B. Cliatt, A. Loizos, Incorporation of GPR data into genetic algorithms for assessing recycled pavements, Constr. Build. Mater. 154 (2017) 1263–1271.
[30] S.L. Lu, M. Li, M.L. Liu, Design of power windows based on POWERLINK industrial Ethernet, Applied Mechanics and Materials, Vol. 494, Trans Tech Publications, 2014, pp. 28–31.
[31] Z. Tong, J. Gao, H. Zhang, Innovative method for recognizing subgrade defects based on a convolutional neural network, Constr. Build. Mater. 169 (2018) 69–82.
[32] Z. Tong, J. Gao, H. Zhang, Recognition, location, measurement, and 3D reconstruction of concealed cracks using convolutional neural networks, Constr. Build. Mater. 146 (2017) 775–787.
[33] Tong, Zheng. Research on pavement distress inspection based on deep learning and ground penetrating radar. Chang'an University, Xi'an, China.
[34] A. Sha, R. Cai, J. Gao, Research on subgrade distresses recognition based on convolutional neural network, J. Chang'an Univ. (Natural Sci. Ed.) 02 (2019) 156–166.
[35] A.P. Annan, Ground Penetrating Radar: Principles, Procedures & Applications, Sensors and Software Inc, Canada, 2003.
[36] I. Goodfellow, Y. Bengio, A. Courville, Deep Learning, MIT press, 2016.
[37] J.T. Springenberg, A. Dosovitskiy, T. Brox, M. Riedmiller. Striving for simplicity: The all convolutional net. arXiv preprint arXiv:1412.6806, (2014).
[38] A. Krizhevsky, I. Sutskever, G.E. Hinton, Imagenet classification with deep convolutional neural networks, in: Advances in Neural Information Processing Systems, 2012, pp. 1097–1105.
[39] I.J. Goodfellow, D. Warde-Farley, M. Mirza, A. Courville, Y. Bengio. Maxout networks. arXiv preprint arXiv:1302.4389, (2013).
[40] N. Srivastava, G. Hinton, A. Krizhevsky, I. Sutskever, R. Salakhutdinov, Dropout: a simple way to prevent neural networks from overfitting, J. Mach. Learn. Res. 15 (1) (2014) 1929–1958.
[41] M. Lin, Q. Chen, S. Yan. Network in network. arXiv preprint arXiv:1312.4400, (2013).
[42] L. Bottou, Large-scale machine learning with stochastic gradient descent, in: Proceedings of COMPSTAT'2010, Physica-Verlag HD, 2010, pp. 177–186.
[43] D. Mishkin, J. Matas. All you need is a good init. arXiv preprint arXiv:1511.06422, (2015).
[44] JTG H20–2007, Highway Performance Assessment Standards, Beijing, China.